Determining the atomic structure of the (4 × 4) silicene layer on Ag(111) by combined grazing-incidence x-ray diffraction measurements and first-principles calculations

A. Curcella,[1] R. Bernard,[1] Y. Borensztein,[1] A. Resta,[2] M. Lazzeri,[3] and G. Prévot[1,*]

[1]*Sorbonne Universités, UPMC Univ Paris 06, CNRS-UMR 7588, Institut des NanoSciences de Paris, F-75005, Paris, France*

[2]*Synchrotron SOLEIL, L'Orme des Merisiers Saint-Aubin–BP 48 91192 Gif-sur-Yvette CEDEX*

[3]*Sorbonne Universités, UPMC Univ Paris 06, CNRS-UMR 7590, MNHN, IRD UMR 206, Institut de Minéralogie, de Physique des Matériaux et de Cosmochimie, F-75005, Paris, France*

(Received 20 July 2016; revised manuscript received 5 October 2016; published 25 October 2016)

From grazing-incidence x-ray diffraction measurements and density functional theory calculations, we have precisely determined the atomic positions of the Si and Ag atoms forming the (4 × 4) Si/Ag(111) silicene reconstruction. A remarkable agreement is found between the experimental structure factors and the theoretical ones derived from the calculations. Our results confirm the honeycomb structure previously proposed, with a buckling of Si atoms equal to 0.77 Å. The Ag substrate atoms are also relaxed, leading to a nonnegligible elastic deformation energy of the substrate, equal to 43 mJ/m^2.

DOI: 10.1103/PhysRevB.94.165438

I. INTRODUCTION

The advent of graphene [1,2] has triggered an increasing interest in the research of two-dimensional (2D) materials in the last decade. Silicene, the 2D allotrope of silicon, has attracted much attention, since pioneer density functional theory (DFT) studies [3,4] have predicted metastable configurations for this material. Indeed, in the so-called free-standing silicene (FSS), silicon atoms arrange themselves in an hexagonal low-buckled structure, in which the vertical distortion is related to a mixed sp^2-sp^3 hybridization [5]. Concerning the electronic properties, FSS is expected to show "Dirac cones" at the K-K′ points of the Brillouin zone, i.e., linear electronic band dispersion, as in graphene. This feature would make silicene very attractive for possible technological applications [6,7], with the advantage of being compatible with the current silicon-based microelectronics. Experimentally, 2D silicon structures have been reported to grow onto different substrates, such as ZrB_2(0001) [8], Ir(111) [9], and MoS_2 [10]. Nevertheless, most of the studies have been performed on Ag(111) and Ag(110) [5,11–26]. Silver appears to be appropriate for silicene growth since: (i) the Ag-Si phase diagram shows nonmiscibility of the solid phases, (ii) Ag and Si lattice constants are in 3/4 ratio, and (iii) their similar electronegativity should result in a small charge transfer between the Si layer and the substrate. However, joint experimental studies and DFT calculations have revealed a nonnegligible interaction between Si and Ag [24,27–31], which results in the loss of the electronic properties predicted for the FSS. Depending on both deposition rate and temperature [15,16,19,27], different ordered superstructures form after one monolayer (ML) deposition on a Ag(111) substrate: (4 × 4) [5,14–21,23,25], $(\sqrt{13} \times \sqrt{13})R13.9^\circ$ [14,15,17,19,21,23,25], $(2\sqrt{3} \times 2\sqrt{3})$R30° [12,14,16,25], (3.5 × 3.5) R26° [19], and $(\sqrt{7} \times \sqrt{7})$R19.1° [14,21]. Each of these structures has been interpreted as a single silicon layer, arranged in an honeycomb lattice, with distinct orientations. The reported Si-Si distances are close to the one predicted for FSS. Moreover, after evaporating more than 1 ML, it has been noticed that the appearance of the second monolayer comes along with the observation of an additional $(4/\sqrt{3} \times 4/\sqrt{3})$R30° reconstruction [13,19], which remains visible also at higher coverages and for which a stability of the film in air has been claimed [32]. Such thick Si films were first addressed to as "multilayer silicene"; however, further studies revealed their diamond bulklike structure and the surfactant behavior of silver atoms [33–35]. The determination of the atomic structure of the reconstructions is of profound interest, being closely related to the electronic bands simulated by DFT calculation. Exploiting combined scanning tunneling microscopy (STM) and DFT calculations, two models have been proposed for the (4 × 4) superstructure, which grows on Ag(111). Independently, Lin *et al.* [17] and Vogt *et al.* [18] came up with a honeycomb structure whose unit cell comprises 18 atoms, 6 of which laying above the plane common to the other 12 atoms. This model has been found to be in agreement also with atomic force microscopy (AFM) results [20,21]. On the other hand, Feng *et al.* [15] proposed a unit cell with a much lower Si density, i.e., 12 Si atoms per unit cell. Eventually, quantitative low-energy electron diffraction (LEED) [24] and reflection high-energy positron diffraction (RHEPD) [22] confirmed the first model and reported values for the deduced buckling, Si-Si distances, bond angles and substrate relaxation. On the contrary, a third model with one added Ag atom per unit cell has been recently proposed on the basis of extended x-ray adsorption fine structure (EXAFS) measurements [36]. However, the interpretation of EXAFS is difficult for the (4 × 4) superstructure due to the large number of atoms in nonequivalent positions. Likewise, the quantitative interpretation of LEED and RHEPD measurements is complicated because of multiple scattering effects. Moreover, these last techniques are mainly sensitive to the very first atomic planes, which results in a low precision on the substrate relaxations. On the contrary, grazing incidence x-ray diffraction (GIXD) is well described by the kinematic theory and is sensitive to both the substrate

*geoffroy.prevot@insp.jussieu.fr

 ©2016 American Physical Society

relaxations and the atomic positions of the overlayer. In this paper we present experimental GIXD and theoretical DFT results which lead to the precise determination of the structure of the (4 × 4) silicene layer. A remarkable agreement is found between the experimental structure factors and the theoretical ones derived from the calculations in the framework of a honeycomb silicene layer. Further DFT calculations show that the presence of the silicene layer induces a significant strain on surface Ag atoms that propagate into the substrate.

II. EXPERIMENTAL AND COMPUTATIONAL DETAILS

GIXD experiments have been performed on the SIXS beamline of SOLEIL synchrotron facility, by using monochromatic x rays of 18.46 keV photon energy. The incident beam has been kept at an angle of 0.145° in order to reduce both the penetration depth of incoming x rays and the bulk diffuse scattering. The sample, a Ag(111) single crystal, was prepared by a few cycles of Ar^+ sputtering ($P = 7 \times 10^{-5}$ mbar, 700 eV) and annealing ($T = 870$ K), in an ultrahigh vacuum (UHV) chamber, with a base pressure around 10^{-10} mbar. Silicon deposition was performed keeping the Ag substrate at either $T = 520$ K or $T = 570$ K. Si was evaporated with an Omicron Nanotechnology e-beam evaporator; the deposition rate was 1 ML/2700 s, as estimated by surface differential reflectance spectroscopy measurements (see Supplemental Material of Ref. [35]). In the present case, 1 ML corresponds to the completion of a (4 × 4) silicene layer, referring to the model proposed by Vogt *et al.* [18]: 18 Si atoms are placed onto a (4 × 4) silver cell, resulting in an atomic Si density of 1.56×10^{15} atoms/cm^2. The unit cell of the (4 × 4) reconstruction is used as reference for GIXD results; the corresponding vectors expressed in the hexagonal basis of the Ag(111) surface are $\mathbf{a} = (4a_{Ag}/\sqrt{2},0,0)$, $\mathbf{b} = (0,4a_{Ag}/\sqrt{2},0)$, $\mathbf{c} = (0,0,\sqrt{3}a_{Ag})$, with $a_{Ag} = 4.085$ Å.

The theoretical model proposed in the present work was obtained by DFT simulations as implemented in the QUANTUM ESPRESSO package [37]. Calculations were performed within the framework of three different approximations: local density approximation (LDA) [38], generalized gradient approximation (GGA) [39], and GGA including eventually phenomenological van der Waals corrections (GGA+vdW) [40,41]. The electron-ion interaction is taken into account according to the projector-augmented wave method [42]. The energy cutoff for the plane waves and for the charge was set at 25 and 200 Ry, respectively. The smearing approach described by Marzari and Vanderbilt [43] was used with a broadening of 0.05 Ry. The system was simulated by an input slab consisting of either six or four layers of a (4 × 4) Ag(111) cell, with on top of it the silicene honeycomb structure [18]. A volume of vacuum, with same thickness as six Ag layers, capped the structure. Electronic k-point sampling was done with a 3 × 3 × 1 grid. Atomic positions were relaxed until atomic forces were less than 10^{-3} Ryd/Bohr by keeping fixed the bottom Ag layer (the

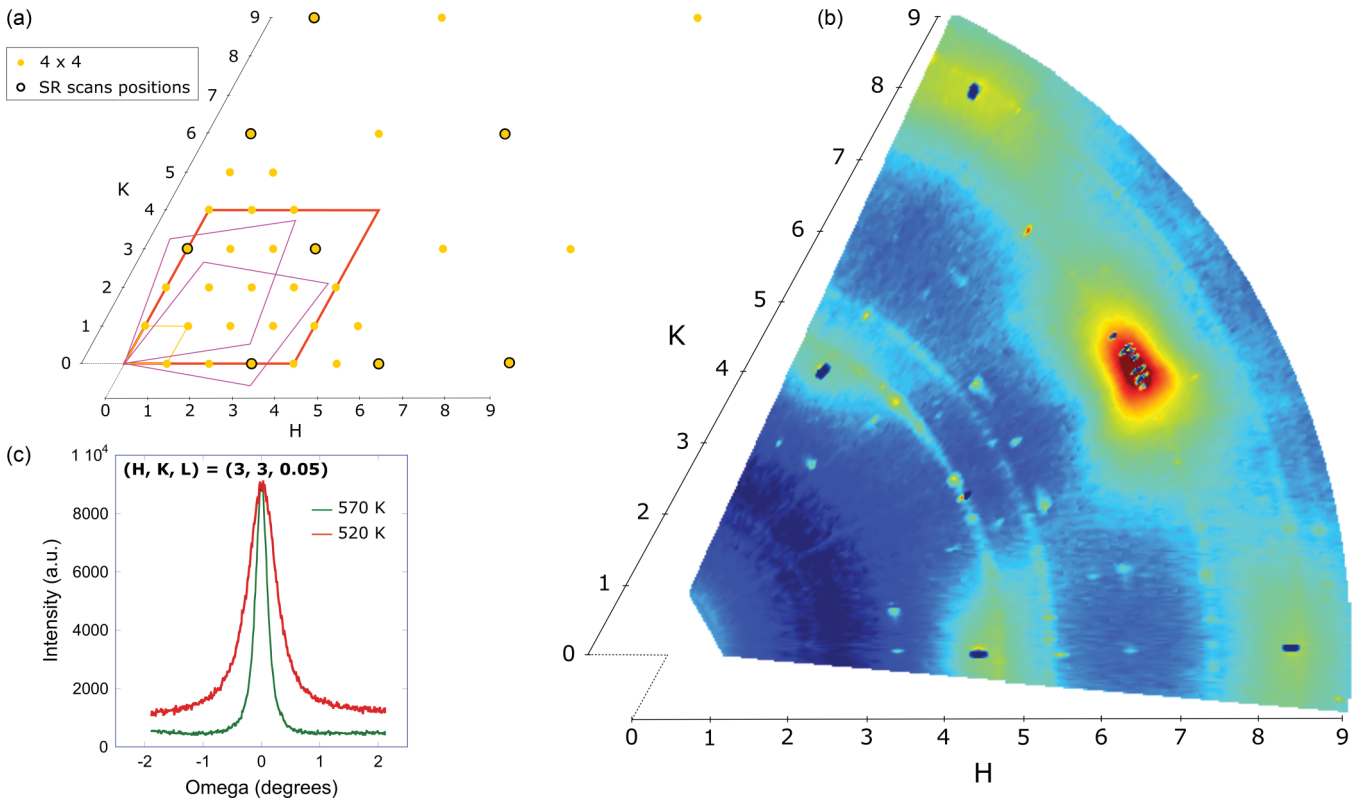

FIG. 1. (a) Schematics of the measurements performed at 520 and 570 K. The indexing of the axis refers to the (4 × 4) reconstruction. The yellow, pink, and red parallelogram represent the (4 × 4), (1.338 × 1.338)$R \pm 10.02°$, and Ag(111) unit cells, respectively. Yellow disks indicate the position of in-plane rocking scans, whereas black circles indicate the position of the analyzed rods. (b) In-plane map ($L = 0.05$) of the reciprocal space obtained by GIXD measurements at 570 K. (c) Rocking scan performed around $(H,K,L) = (3,3,0.05)$ at 520 K (red line) and 570 K (blue line). The almost identical intensity at $\omega = 0$ is fortuitous.

in-plane lattice spacing was kept fixed at the corresponding theoretical bulk equilibrium value). The reference in-plane lattice spacing for bulk Ag is 2.837 Å and 2.935 Å, in the LDA and GGA case, respectively; experimentally the reference value is 2.899 Å. Accounting for vdW corrections does not change the value of the equilibrium lattice constant. At the surface the relaxed structure does not present any relevant difference by changing from four to six Ag layers: hereafter, we will refer to the simulation with six substrate layers, for which the elastic deformation of the substrate should be better described. The resulting surface structure does not substantially change by using 30/240 Ry cutoff, 0.025 Ry smearing, and a $6 \times 6 \times 1$ k-point grid.

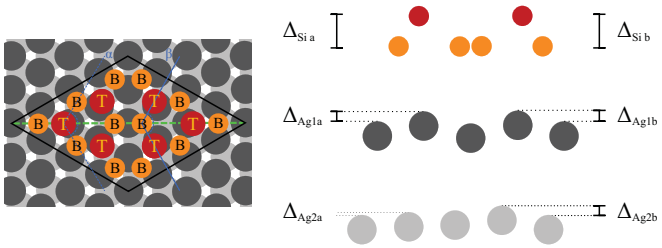

FIG. 2. Top and lateral view of the (4×4) reconstruction on Ag(111), showing the corresponding unit-cell (black parallelogram), the top-lying (T atoms, red), and bottom-lying (B atoms, orange) Si atoms, first and second layer Ag atoms (dark and light grey dots), and the angles between the atoms of the superstructure (α and β).

III. RESULTS

After evaporation of 1 ML of Si, various superstructures coexist on the Ag(111) substrate. The diffracted intensity for in-plane conditions ($L = 0.05$) is shown in Fig. 1(b) for 1 ML of Si evaporation at 570 K. At this temperature, the most intense diffraction spots are associated with a $(1.338 \times 1.338)R \pm 10.02^\circ$ reconstruction, which corresponds to a small distortion of the $(2\sqrt{3} \times 2\sqrt{3})R30^\circ$ superstructure usually observed at high temperature [44,45]. Spots of the (4×4) structure are also visible, with a lower intensity. On the contrary, for deposition at 520 K, the most intense signal comes from the (4×4) structure, whereas the $(\sqrt{13} \times \sqrt{13})R13.9^\circ$ reconstruction is also visible. In the following, we focus on the diffracted intensity associated with the (4×4) superstructure only.

For both temperatures, the intensity of the in-plane (4×4) reflections has been acquired by performing 35 angular rocking scans, in the (H,K) positions shown in Fig. 1(a). In Fig. 1(c) is shown the comparison between the (3, 3, 0.05) spot relative to the (4×4) structure at 520 and 570 K. At the lower temperature, the peak is 2.5 times broader and its integral is 2.4 times higher: the domains of the (4×4) are smaller but cover a higher percentage of the surface. Furthermore, we performed rocking scans at consecutive values of L along several superstructure rods; their corresponding (H,K) positions are indicated as black circles in the schematics of Fig. 1(a). Note that whereas the crystal truncation rods carry the contributions of the various Si domains characterized by different orientations, the analyzed superstructure rods are exclusively associated to the (4×4) reconstruction. This situation is ensured at 570 K by the distortion of the $(2\sqrt{3} \times 2\sqrt{3})$ phase: the theoretical size and orientation would cause some of its spots to superpose with those of the (4×4) reconstruction, which is not the case for the observed structure. At 520 K the two coexistent reconstructions, i.e., (4×4) and $(\sqrt{13} \times \sqrt{13})R13.9^\circ$, have no superposing spots, except of course at the nodes of the Ag(111) surface lattice. The details of the structure factor determination from the raw measurements and the corrections applied [46] are given in the Supplemental Material [47]. Within a scale factor, no remarkable difference has been observed between the results obtained at 520 and 570 K (see Supplemental Material Fig. S1 [47]).

The results of DFT calculations of the (4×4) Si reconstruction on Ag(111), simulated as described in the previous paragraph, give the theoretical atomic positions for both the silicene structure and the Ag substrate. A schematic representation of the system is reported in Fig. 2. Similar results are obtained for the three approximations used (LDA, GGA, vdW). The buckling of the layer, the range of Si bond lengths and the bond angles are reported in Table I, together with previous experimental and theoretical works. For clarity, all theoretical distances have been scaled to the experimental lattice constant. Among the various values computed, the buckling of the Si layer is the more sensitive to the choice of DFT approximation. Whereas a value of $\Delta_{Si} = 0.77$ Å is obtained within the GGA, which is close to the buckling of a bulk Si(111) biplane (0.78 Å), a significantly higher value of 0.90/0.91 Å is obtained within the LDA. This can be related to the different mismatch between Si and Ag bulk lattice constant $f = a_{\mathrm{Si}}/a_{\mathrm{Ag}}$ computed by the two methods. Whereas $f_{\mathrm{GGA}} = 1.3171$ is close to the experimental value $f_{\mathrm{exp}} = 1.3295$, $f_{\mathrm{LDA}} = 1.3467$ is larger. The associated

TABLE I. Comparison between the relevant structure parameters obtained in this work and those available in literature, from DFT calculations or experiments. The present DFT-GGA calculations can be considered as the best fit to GIXD measurements.

		d (Å)	$\Delta_{\mathrm{Si}\,a/b}$ (Å)	$\Delta_{\mathrm{Ag}\,1a/b}$ (Å)	$\Delta_{\mathrm{Ag}\,2a/b}$ (Å)	α	β
Free-standing silicene	DFT-LDA [4]	2.25	0.44				
	DFT-GGA [49]	2.35	0.8	0.4			
	DFT-GGA [18]	2.32	0.75			110°	118°
	LEED [24]	2.29–2.31	0.77/0.74	0.29/0.31	0.10/0.21		
(4×4) Si/Ag(111)	RHEPD [22]		0.83			112°	119°
	DFT-GGA/GIXD	2.30–2.33	0.76	0.25/0.27	0.05/0.24	108.6°	111.1°
	DFT-GGA+vdW	2.30–2.34	0.78/0.79	0.23/0.25	0.04/0.17	108.0°	110.5°
	DFT-LDA	2.33–2.37	0.90/0.91	0.29/0.32	0.07/0.27	105.6°	109.3°

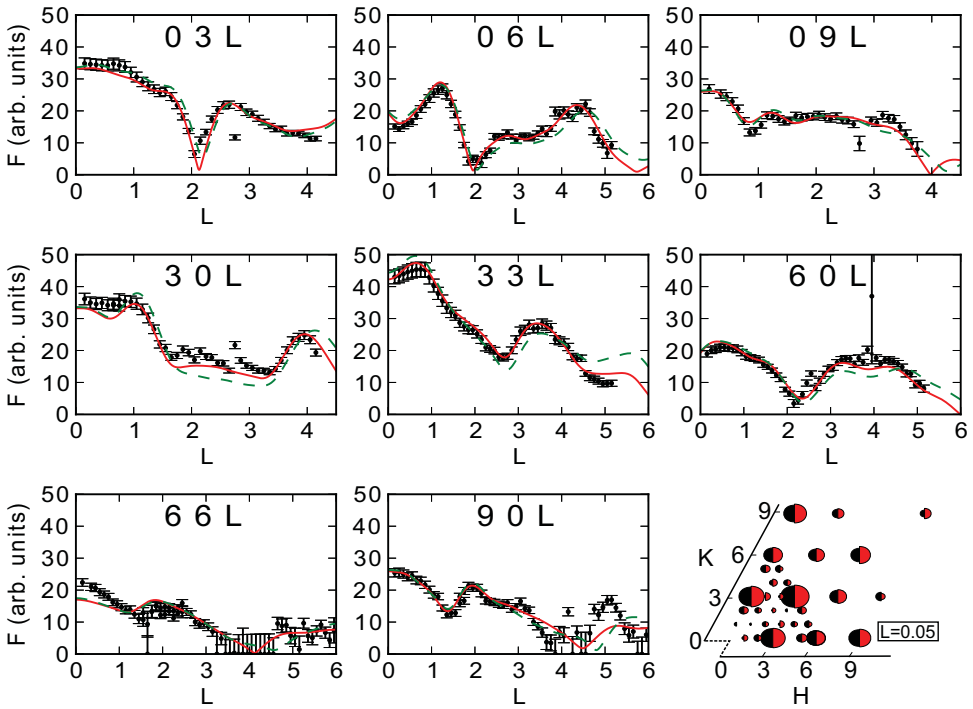

FIG. 3. Comparison between experimental, for $T = 520$ K (black dots with error bars and black half-disks), GGA-simulated (red continuous line and red half-disks), and LDA-simulated (green dotted line) structure factors, along several superstructure rods and for in-plane diffraction conditions ($L = 0.05$).

compressive stress induces thus a higher buckling of the Si layer. In the GGA, the silicon bond lengths obtained are in the 2.30–2.34 Å range, which is in between the expected Si-Si length in free-standing silicene (2.25 Å) and the Si-Si nearest-neighbor distance in bulk Si (2.35 Å). The whole set of bond lengths is shown in Supplemental Material Fig. S2 [47]. The bond angles carry information about the hybridization state of the Si sheet: $\alpha = 108.6^\circ$ is slightly smaller than ideal value of 109.5° for a pure sp^3 hybridized system, while $\beta = 111.1^\circ$ is somewhat bigger. Both angles are far from 120°, suggesting that the hybridization should be much closer to sp_3 than to sp_2. Related to the higher buckling of the Si layer, the α and β angles are found even lower in the LDA. Concerning the substrate, the silicene buckled structure induces a deformation of the topmost Ag layers. Hereby, the silver atoms right below the top-lying Si atoms (orange spots in Fig. 2) are pulled off the plane about $\Delta_{Ag1a} = 0.25$ Å and $\Delta_{Ag1b} = 0.27$ Å, for the left and right half of the (4×4) unit cell, respectively, in GGA results. The deformation affects also the second Ag layer ($\Delta_{Ag2a} = 0.05$ Å, $\Delta_{Ag2b} = 0.24$ Å) and becomes less and less important deeper beneath the surface. As can be seen in Table I, these results are not very sensitive to the kind of approximation chosen. In-plane relaxations of Ag atoms also occurs, but with an amplitude smaller than for out-of-plane relaxations. They are larger in the second Ag plane than in the first one. The evolution with depth of the root-mean-square displacements is shown in Supplemental material Fig. S2 [47]. They decay exponentially in the bulk. The associated decay lengths are $\lambda_{//} = 3.58$ Å for in-plane displacements and $\lambda_\perp = 3.07$ Å for out-of-plane displacements. Such values are two times higher than the value $1/k = 1.59$ Å expected for isotropic crystals, where k is the wave-vector associated with the reconstruction. Such difference is due to the high crystalline anisotropy of Ag [48]. These results and the comparison with previous experimental and theoretical works are reported in Table I. The complete list of atomic coordinates is given in the Supplemental Material [47].

From the atomic positions determined by DFT, we have computed the structure factors for the experimental conditions, in the kinematic theory. As free parameters, we have used only a scale factor and in-plane and out-of-plane Debye-Waller factors; for the Si atoms, the surface Ag atoms and the other Ag atoms. The agreement between experimental (F_{exp}) and simulated (F_{th}) structure factors is estimated by the value of

$$\chi^2 = \frac{1}{N_{pts} - N_{par}} \sum^{N_{pts}} \left(\frac{F_{th} - F_{exp}}{\sigma_{exp}} \right)^2, \qquad (1)$$

where N_{pts} is the number of experimental structure factors, and N_{par}=7 is the number of free parameters. As shown in Fig. 3, there is a remarkable agreement between experiment and theory. Although the theoretical rods look quite similar, the agreement is better for simple GGA calculations ($\chi^2_{GGA} = 5.3$) than for GGA+vdW ($\chi^2_{vdW} = 7.5$) or LDA calculations ($\chi^2_{LDA} = 9.9$). Due to the large number of Si and Ag atoms involved in the structure of the diffracting unit cell, performing a further fit of the data with all atomic positions free to move is meaningless. We can thus consider GGA positions as our best fit to measurements. Notice that, besides the χ^2 analysis, a visual comparison of the theoretical structure factors (Fig. 1 and Supplemental Material Fig. S3 [47]) with measured ones confirms the fact that simple GGA provides a better structure than GGA+vdW (in spite of the fact that vdW corrections are supposed to improve GGA). Notice, also, that GGA and

GGA+vdW structures are very similar (Table I) and that it would be hard to discriminate between the two structures on the sole basis of available LEED measurements.

In conclusion, we clearly confirm that the (4×4) silicene reconstruction corresponds to a buckled honeycomb layer, as proposed by Vogt *et al.* [18]. GIXD not only confirms the atomistic model of the (4×4) silicene structure, it also shows that the Ag substrate is strongly relaxed upon Si adsorption. Whereas the Si layer has an almost perfect hexagonal symmetry, the superstructure diffraction rods have clearly a trigonal symmetry. For example, the $(0\ 3\ L)$ and $(3\ 0\ L)$ rods are markedly different. This is due to the different contributions from Ag substrate atoms for which the symmetry is trigonal. As already mentioned, the relaxations of surface Ag atoms propagate elastically into the bulk with an exponential decay. GIXD is sensitive to these elastic relaxation modes that give specific contributions to the superstructure rods [50]. They correspond for example to the peaks near $L = 1$ on the $(3\ 0\ L)$ and $(0\ 6\ L)$ rods, to the peak near $L = 2$ on the $(9\ 0\ L)$ rod and to the dip at $L = 2$ on the $(0\ 3\ L)$ rod. The very good agreement between experiment and theory allows us to estimate the elastic deformation energy of the Ag substrate. For this purpose, we have computed within DFT the energy of the Ag surface when it is stripped of the Si atoms (without further relaxation). This energy carries information on the silicene-induced deformation of the Ag substrate and can be compared with the energy of a fully relaxed clean Ag surface. The difference between the two energies represents the elastic energy of the Ag substrate, induced by the silicene sheet. The value per Ag atom is 43 mJ/m^2, which is small if compared to Ag surface energy 1.25 J/m^2 [51]. It is, however, much higher, for example, than the elastic substrate deformation energy measured for oxygen adsorbed on Cu(110) (10^{-3} J/m^2), which is responsible of the self-organization of Cu-O stripes at the Cu crystal surface [52]. This indicates that the silicene layer markedly interacts with the Ag surface.

IV. CONCLUSIONS

In summary, we have precisely determined the structure of the (4×4) silicene layer grown on the Ag(111) surface. An impressive agreement between GIXD measurements and DFT simulations in the GGA is found. Our comparison shows thus that GGA is more suited for the Ag-Si system than LDA. We not only validate the model of a buckled honeycomb structure previously proposed, but we also precisely determine the atomic buckling of the layer, equal to 0.76 Å, the different Si bond lengths and angles, and the atomic positions of the Ag atoms near the surface. Indeed, Ag atoms, due to their important relaxations, give a nonnegligible contribution to the diffracted intensity. We have computed the associated elastic deformation energy, which is found equal to 43 mJ/m^2.

ACKNOWLEDGMENTS

This work was supported by French state funds managed by the ANR within the Investissements d'Avenir program under Reference No. ANR-11-IDEX-0004-02 and more specifically within the framework of the Cluster of Excellence MATISSE. The SIXS beamline staff is greatly acknowledged for the technical support.

[1] A. K. Geim, Science **324**, 1530 (2009).
[2] A. K. Geim and K. S. Novoselov, Nat. Mater. **6**, 183 (2007).
[3] K. Takeda and K. Shiraishi, Phys. Rev. B **50**, 14916 (1994).
[4] S. Cahangirov, M. Topsakal, E. Aktürk, H. Şahin, and S. Ciraci, Phys. Rev. Lett. **102**, 236804 (2009).
[5] E. Cinquanta, E. Scalise, D. Chiappe, C. Grazianetti, B. van den Broek, M. Houssa, M. Fanciulli, and A. Molle, J. Phys. Chem. C **117**, 16719 (2013).
[6] Z. Ni, H. Zhong, X. Jiang, R. Quhe, G. Luo, Y. Wang, M. Ye, J. Yang, J. Shi, and J. Lu, Nanoscale **6**, 7609 (2014).
[7] L. Tao, E. Cinquanta, D. Chiappe, C. Grazianetti, M. Fanciulli, M. Dubey, A. Molle, and D. Akinwande, Nature Nanotechnol. **10**, 227 (2015).
[8] A. Fleurence, R. Friedlein, T. Ozaki, H. Kawai, Y. Wang, and Y. Yamada-Takamura, Phys. Rev. Lett. **108**, 245501 (2012).
[9] L. Meng, Y. Wang, L. Zhang, S. Du, R. Wu, L. Li, Y. Zhang, G. Li, H. Zhou, W. A. Hofer, and H.-J. Gao, Nano Lett. **13**, 685 (2013).
[10] D. Chiappe, E. Scalise, E. Cinquanta, C. Grazianetti, B. van den Broek, M. Fanciulli, M. Houssa, and A. Molle, Adv. Mater. **26**, 2096 (2014).
[11] B. Aufray, A. Kara, S. Vizzini, H. Oughaddou, C. Landri, B. Ealet, and G. Le Lay, Appl. Phys. Lett. **96**, 183102 (2010).
[12] B. Lalmi, H. Oughaddou, H. Enriquez, A. Kara, S. Vizzini, B. Ealet, and B. Aufray, Appl. Phys. Lett. **97**, 223109 (2010).
[13] L. Chen, C.-C. Liu, B. Feng, X. He, P. Cheng, Z. Ding, S. Meng, Y. Yao, and K. Wu, Phys. Rev. Lett. **109**, 056804 (2012).
[14] D. Chiappe, C. Grazianetti, G. Tallarida, M. Fanciulli, and A. Molle, Adv. Mater. **24**, 5088 (2012).
[15] B. Feng, Z. Ding, S. Meng, Y. Yao, X. He, P. Cheng, L. Chen, and K. Wu, Nano Lett. **12**, 3507 (2012).
[16] H. Jamgotchian, Y. Colignon, N. Hamzaoui, B. Ealet, J. Y. Hoarau, B. Aufray, and J. P. Bibrian, J. Phys.: Condens. Matter **24**, 172001 (2012).
[17] C.-L. Lin, R. Arafune, K. Kawahara, Noriyuki Tsukahara, E. Minamitani, Y. Kim, N. Takagi, and M. Kawai, Appl. Phys. Express **5**, 045802 (2012).
[18] P. Vogt, P. De Padova, C. Quaresima, J. Avila, E. Frantzeskakis, M. C. Asensio, A. Resta, B. Ealet, and G. Le Lay, Phys. Rev. Lett. **108**, 155501 (2012).
[19] R. Arafune, C.-L. Lin, K. Kawahara, Noriyuki Tsukahara, E. Minamitani, Y. Kim, N. Takagi, and M. Kawai, Surf. Sci. **608**, 297 (2013).
[20] Z. Majzik, M. Rachid Tchalala, M. Švec, P. Hapala, H. Enriquez, A. Kara, A. J. Mayne, G. Dujardin, P. Jelínek, and H. Oughaddou, J. Phys.: Condens. Matter **25**, 225301 (2013).

[21] A. Resta, T. Leoni, C. Barth, A. Ranguis, C. Becker, T. Bruhn, P. Vogt, and G. Le Lay, Sci. Rep. **3**, 2399 (2013).
[22] Y. Fukaya, I. Mochizuki, M. Maekawa, K. Wada, T. Hyodo, I. Matsuda, and A. Kawasuso, Phys. Rev. B **88**, 205413 (2013).
[23] C. Grazianetti, D. Chiappe, E. Cinquanta, G. Tallarida, M. Fanciulli, and A. Molle, Appl. Surf. Sci. **291**, 109 (2014).
[24] K. Kawahara, T. Shirasawa, R. Arafune, C.-L. Lin, T. Takahashi, M. Kawai, and N. Takagi, Surf. Sci. **623**, 25 (2014).
[25] P. Moras, T. O. Mentes, P. M. Sheverdyaeva, A. Locatelli, and C. Carbone, J. Phys.: Condens. Matter **26**, 185001 (2014).
[26] M. R. Tchalala, H. Enriquez, A. J. Mayne, A. Kara, G. Dujardin, M. A. Ali, and H. Oughaddou, J. Phys.: Conf. Ser. **491**, 012002 (2014).
[27] R. Bernard, Y. Borensztein, H. Cruguel, M. Lazzeri, and G. Prévot, Phys. Rev. B **92**, 045415 (2015).
[28] G. Prévot, R. Bernard, H. Cruguel, and Y. Borensztein, Appl. Phys. Lett. **105**, 213106 (2014).
[29] C.-L. Lin, R. Arafune, K. Kawahara, M. Kanno, N. Tsukahara, E. Minamitani, Y. Kim, M. Kawai, and N. Takagi, Phys. Rev. Lett. **110**, 076801 (2013).
[30] S. K. Mahatha, P. Moras, V. Bellini, P. M. Sheverdyaeva, C. Struzzi, L. Petaccia, and C. Carbone, Phys. Rev. B **89**, 201416 (2014).
[31] N. W. Johnson, P. Vogt, A. Resta, P. De Padova, I. Perez, D. Muir, E. Z. Kurmaev, G. Le Lay, and A. Moewes, Adv. Funct. Mater. **24**, 5253 (2014).
[32] P. De Padova, C. Ottaviani, C. Quaresima, B. Olivieri, P. Imperatori, E. Salomon, T. Angot, L. Quagliano, C. Romano, A. Vona, M. Muniz-Miranda, A. Generosi, B. Paci, and G. Le Lay, 2D Mater. **1**, 021003 (2014).
[33] A. J. Mannix, B. Kiraly, B. L. Fisher, M. C. Hersam, and N. P. Guisinger, ACS Nano **8**, 7538 (2014).
[34] T. Shirai, T. Shirasawa, T. Hirahara, N. Fukui, T. Takahashi, and S. Hasegawa, Phys. Rev. B **89**, 241403 (2014).
[35] Y. Borensztein, A. Curcella, S. Royer, and G. Prévot, Phys. Rev. B **92**, 155407 (2015).
[36] P. Lagarde, M. Chorro, D. Roy, and N. Trcera, J. Phys.: Condens. Matter **28**, 075002 (2016).
[37] P. Giannozzi, S. Baroni, N. Bonini, M. Calandra, R. Car, C. Cavazzoni, D. Ceresoli, G. L. Chiarotti, M. Cococcioni, I. Dabo, A. Dal Corso, S. de Gironcoli, S. Fabris, G. Fratesi, R. Gebauer, U. Gerstmann, C. Gougoussis, A. Kokalj, M. Lazzeri, L. Martin-Samos, N. Marzari, F. Mauri, R. Mazzarello, S. Paolini, A. Pasquarello, L. Paulatto, C. Sbraccia, S. Scandolo, G. Sclauzero, A. P. Seitsonen, A. Smogunov, P. Umari, and R. M. Wentzcovitch, J. Phys.: Condens. Matter **21**, 395502 (2009).
[38] J. P. Perdew and A. Zunger, Phys. Rev. B **23**, 5048 (1981).
[39] J. P. Perdew, K. Burke, and M. Ernzerhof, Phys. Rev. Lett. **77**, 3865 (1996).
[40] S. Grimme, J. Comput. Chem. **27**, 1787 (2006).
[41] V. Barone, M. Casarin, D. Forrer, M. Pavone, M. Sambi, and A. Vittadini, J. Comput. Chem. **30**, 934 (2009).
[42] G. Kresse and D. Joubert, Phys. Rev. B **59**, 1758 (1999).
[43] N. Marzari, D. Vanderbilt, A. De Vita, and M. C. Payne, Phys. Rev. Lett. **82**, 3296 (1999).
[44] H. Jamgotchian, B. Ealet, Y. Colignon, H. Maradj, J.-Y. Hoarau, J.-P. Biberian, and B. Aufray, J. Phys.: Condens. Matter **27**, 395002 (2015).
[45] M. S. Rahman, T. Nakagawa, and S. Mizuno, Jpn. J. Appl. Phys. **54**, 015502 (2015).
[46] O. Robach, Y. Garreau, K. Ad, and M. B. Vron-Jolliot, J. Appl. Crystallogr. **33**, 1006 (2000).
[47] See Supplemental Material at http://link.aps.org/supplemental/10.1103/PhysRevB.94.165438 for details of the structure factor determination from raw measurements and corrections applied.
[48] B. Croset and G. Prévot, Phys. Rev. B **73**, 045434 (2006).
[49] H. Enriquez, A. Kara, A. J. Mayne, G. Dujardin, H. Jamgotchian, B. Aufray, and H. Oughaddou, J. Phys.: Conf. Ser. **491**, 012004 (2014).
[50] G. Prévot, A. Coati, B. Croset, and Y. Garreau, J. Appl. Crystallogr. **40**, 874 (2007).
[51] L. Vitos, A. Ruban, H. Skriver, and J. Kollr, Surf. Sci. **411**, 186 (1998).
[52] G. Prévot, B. Croset, Y. Girard, A. Coati, Y. Garreau, M. Hohage, L. Sun, and P. Zeppenfeld, Surf. Sci. **549**, 52 (2004).